Eco-safe chemicothermal conversion of industrial graphite waste to exfoliated graphene and evaluation as engineered adsorbent to remove toxic textile dyes

Selvaraj Ambika [a,*], Valasani Srilekha [b]

[a] *Assistant Professor, Department of Civil Engineering, Indian Institute of Technology Hyderabad, India 502285*
[b] *National Institute of Technology Warangal, India*

ARTICLE INFO

ABSTRACT

Industrial graphite becomes waste after its use and dumping of such graphite waste leads to environmental damage and health risks, thus needs alternative measures. This study is the first of its kind to convert industrial graphite to exfoliated graphene(EG) and using EG as an adsorbent. The used conversion method is chemicothermal which is greener and competent. The resultant EG was micro-analyzed for its application as an engineered adsorbent. The adsorption capacity of EG is tested for the removal of five toxic dyes from aqueous solution, namely royal blue (RB), turquoise blue (TB), black supra (BS), navy blue (NB), and deep red (DR) for various environmental conditions. The order of adsorption at equilibrium was found to follow, DR > TB > BS > NB > RB at circum-neutral pH in the range of 5 - 25 mg/L of dye, having 0.2 gm of EG. The notable adsorption capacity of dye onto EG can be credited to the various interface mechanisms which were studied using kinetic and thermodynamic models. The reusability studies recommend EG as the alternate adsorbent against commercial activated carbon which holds a huge carbon and water footprint. These results suggest that the applicability of potential EG adsorbent can be extended to the removal of organic pollutants in water and wastewater treatment. The success of converting graphite waste to an engineered dye adsorbent couples the advantages of converting industrial waste to a beneficial product and removal of toxic dyes thus achieving the circular economy and sustainable development in industrial practices.

1. Introduction

The industries are the spine of any country's economic growth and fix the country's status across the world, henceforth it is unavoidable (K. Akatmatsu, 1962).On the other hand, massive industrial waste production causes global environmental threats and hence necessitates the prerequisite balance between the financial benefits and safe environment (Azapagic, 2004; Citation, 1994; Dauvergne and Lister, 2012; Gray and Jan Bebbington, 2001; Langdon et al., 2019; Prăvălie and Bandoc, 2018). Different industries use different raw materials and so the generated waste (Allen and Behmanesh, 1994; Bruvoll and Ibenholt, 1997; Fellner et al., 2017; Pappu et al., 2007; Polprasert and Liyanage, 1996; Sendra et al., 2007; Tsai and Chou, 2004; Wiemes et al., 2017). Among industrial wastes, a large amount of graphite waste is generated from forging industries and refineries (C. Schacht, 2004; C.J.Mitchell, 1992; Dean, 2000; Feytis, 2010; Kryachek, 2004; Lee and Zhang, 1999;

Li et al., 2018; Patterson and Cheng, 1975; R.S.Kalyoncu, 2002; Sutphin et al., 1990; Taylor, 2000; Vorpahl et al., 1976; Wareing et al., 2017). The major uses of graphite are in brake linings, lubricants, powdered metals, refractory applications, and steelmaking. In the global scenario, China took the top spot for graphite mining by having 95,000 MT, with India and Brazil coming in second and third, respectively (Feytis, 2010; R.S.Kalyoncu, 2002; Taylor, 2000). All the mined graphite goes to industry and followed by use, it becomes waste. To date, there is no proper disposal or recycling method for industrial graphite waste is developed because of the abundance of graphite availability (Li et al., 2018; Wareing et al., 2017).

The fate, transformation, and transport of dumped graphite waste in soil, water, and air components root i) environmental issues being as the absorber and carrier of toxic compounds, ii) acute and severe health problems such as graphitosis due to unnecessary graphite exposure and iii) nuisance/inconvenience in the social system because the graphite

dust is dense enough to impede visibility (Kang et al., 2020; Kryachek, 2004; Patterson and Cheng, 1975; Vorpahl et al., 1976). Hence, the life cycle of graphite from its mining, industrial usage followed by its dumping cost huge ecological footprint, societal health damage, and economical loss (Feytis, 2010; R.S.Kalyoncu, 2002; Taylor, 2000). All these effects compel the need for proper graphite waste management options.

Circular economy, sustainable development, and green engineering practices describe the reuse and recycle of different industrial wastes (Allen and Behmanesh, 1994; Bendikiene et al., 2019; Fellner et al., 2017; Tsai and Chou, 2004; Wiemes et al., 2017). In this paper, the studied auto-forging industry, Chennai, India, uses graphite as a lubricant and generates approximately a ton of graphite waste every month. This study investigated the effectiveness of converting spent graphite to a value-added adsorbent and checks its applicability as an adsorbent in pollutant removal.

Graphite-based materials-mediated adsorption is a well-established technique in the past decade. Among, graphite oxide, graphene, graphene oxide, expanded graphene, and exfoliated graphene are being proved as the superior adsorbents (Capone et al., 2019; Duan et al., 2016; Pozzetto et al., 2020; Yang et al., 2019; Yusuf et al., 2015). Having unique chemical, electrical and physical properties, in this study exfoliated graphene (EG)was synthesized from the graphite waste. In recent times, the method of thermal reduction is an effective way of reducing graphene oxide (GO) which is the mid material in EG synthesis from graphite and has been considered as a green technique, because of zero usage of hazardous reductants or chemicals for the chemical reduction (Chen et al., 2010; Gao et al., 2010; Larciprete et al., 2011; Lavin-Lopez et al., 2019; Zhu et al., 2010).

The adsorption performance of the synthesized EG was tested for dye adsorption (Hu et al., 2019; Larciprete et al., 2011; Shittu et al., 2019; Sykam et al., 2018). Given their complex structure and synthetic origin, dyes used in textile industries contribute to 18-20% of the global water pollution, and their toxicity causes health-risks ranging from a skin rash to cancer (A.Reife, 1996; Carmen and Daniel, 2012; Clarke and Anliker, 1980; F.L.Slejko, 1985; Hossain et al., 2018). The adsorption treatment technique garnered popularity due to its simplicity of design, high-cost efficiency, and accelerated removal of pollutants (Hou et al., 2020; Sophia A. and Lima, 2018). Previously, graphite cathode waste which consists of fluoride and cyanide was treated with strong acids or bases to leach the hazardous chemicals that again cause huge environmental impact. Further, it was converted to GO using the Hummers method and tested as an additive in water-based drilling fluids. However, there is no existing study on the synthesis of EG from industrial graphite which does not hold any harmful substances and is trailed as an adsorbent for pollution removal.

As a summary, the focus of this paper is to evaluate the efficiency of dye adsorption using an adsorbent prepared from graphite waste by the eco-friendly method. The tasks involved are 1) synthesis of EG from graphite waste using thermal reduction method 2) characterization of the adsorbent and 3) assess the adsorption efficiency of EG on the removal of dyes from aqueous solution by varying the parameters like solution pH, dye, and sorbent dose, presence of salt, shaking speed and contact time. This attempt of converting industrial graphite waste to a beneficial adsorbent and its performance check against toxic textile dyes is the first of its kind.

2. Materials and method

The spent graphite was collected from an auto forging industry, Chennai, India. All the chemicals used in this study are analytical grade and purchased from Rankem, India. For the adsorbent synthesis and experiments, deionized water was used. All the dyes used are industrial grade and collected from the dye industry, Tirupur, India. Glassware and sample vials were cleaned and washed with deionized water before and after every use.

2.1. Preparation of EG from industrial graphite

The collected spent graphite was washed multiple times to remove the foreign matter and dried at 60°C for 2 h to get rid of the moisture content (2 to 6%) that it grew during the industrial processes. After drying, the industrial spent graphite was sieved using a 20μm sieve and the resultant graphite was converted to GO using modified Hummer's method (Dao and Jeong, 2015; Kaniyoor and Ramaprabhu, 2011; Luo et al., 2017; Xian et al., 2015). The obtained brownish yellow color GO was kept under thermal treatment for its exfoliation and reduction as follows; The samples were taken in a silica crucible and kept in the furnace for 8 h. The activation temperatures were maintained as 500°C, 700°C, 900°C, and 1100°C, and the resultant black color samples were named as exfoliated graphene (EG), EG_{500}, EG_{700}, and EG_{900}, and EG_{1100}, respectively. After cooling down, the EGs were stored in an airtight container till their use in adsorption studies.

2.2. Characterization

The prepared samples were characterized for understanding the change during its preparation. Fourier-transform infrared spectroscopy (FTIR) and X-Ray Diffraction Spectroscopy (XRD) (CuKα, Lynx detector, 35 kV, 25 mA, Bruker Axs, USA) analysis were done to capture the variation in distinct characteristics of graphite's conversion to EG. The change in surface morphology was checked using Scanning Electron Microscopy (SEM) (JEOL, JSM-6380, Japan). The chemical composition was confirmed by Energy-Dispersive X-ray spectroscopy (EDAX) analysis (EDAX; FEI, Quanta 200, Czechoslovakia). The surface area and pore volume were characterized by the N_2 adsorption/desorption isotherm using Brunauer–Emmett–Teller (BET) using micromeritics ASAP 2020. Zeta potential analyzer (Horiba Scientific, SZ-100) was used to find the surface charge of the sample (Temperature of the Holder 25°C, Dispersion Medium Viscosity 0.896 mS/cm, conductivity 0.068 mS/cm, dielectric constant 78.321, electrode voltage 2.7 V) (C.J. Mitchell, 1992; Larciprete et al., 2011; Shittu et al., 2019). The maximum absorption wavelength for the dyes was figured out using the UV-Visible spectrophotometer (UV-1800, Shimadzu Corporation, Japan) for the scan range of 200-900 nm.

2.3. Adsorption experiments and isotherms

The sacrificial mode adsorption experiments were conducted at the base concentration of each dye unless otherwise specified (Chung et al., 2015; Selvanantharajah et al., 2019). The adsorption capacity was tested for the prepared EG at different activation temperatures (0.5 gm of EG_{500}, EG_{700}, EG_{900}, and EG_{1100}, 2 h of contact time), different EG dose (0.2, 0.28, 0.35, 0.42 and 0.5 gm), dye concentration (5, 10, 15, 20 and 25 mg/L), contact time (0, 30, 60, 120 and 180 min), initial pH of the solution (3, 4, 6, 7, 8 and 10), shaking conditions (100, 125, 150, 200, and 230 rpm), and effect of salt (0.1 M NaCl or $MgCl_2$). The initial pH of the solution was changed using 0.1 N HCl or NaOH.

Unless otherwise specified, 15 mg/L dye, 0.2 gm EG dosage, 125 rpm shaking speed of orbital shaker, sampling time of 0, 30, 60, 120, and 180 min, and neutral - initial pH of the solution was maintained. Similar experiments were conducted using commercial grade activated carbon as detailed in the supplementary information.

The dye removal efficiency of EG(R in %) was calculated from equation (1).

$$R = \frac{C_i - C_f}{C_i} \; x \; 100 \tag{1}$$

where C_i and C_f are the initial and final dye concentrations (Desta, 2013; Li et al., 2019).

Langmuir and Freundlich isotherms were used to evaluate the adsorption at equilibrium.
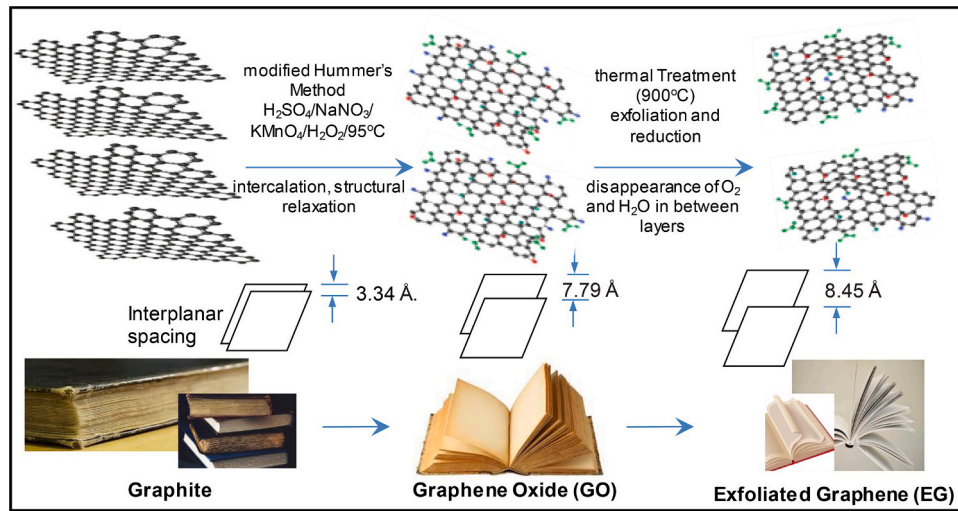
Fig. 1. Conversion mechanism of industrial graphite waste to EG under chemicothermal process

Langmuir equation is given in Eq. (2).

$$\frac{C_e}{q_e} = \frac{1}{q_{max}K_L} + \frac{C_e}{q_{max}} \tag{2}$$

Where, C_e (mg/L)is equilibrium dye concentration, q_e(mg/gm)is the mass of dye removed at equilibrium per unit mass of EG, q_{max} (mg/gm)is the maximum monolayer adsorption capacity of EG and K_L is the Langmuir constant (Desta, 2013; Hossain et al., 2018; Lavin-Lopez et al., 2019; Li et al., 2019; Sophia A. and Lima, 2018; Sykam et al., 2018). The slope and intercept values from the plot of C_e/q_e against C_e, are used to find the values of q_{max} and K_L.

The Freundlich adsorption equation in its linear form is given in Eq. (3).

$$q_e = K_f C_e^{\frac{1}{n}} \tag{3}$$

Here C_e (mg/L) is the concentration of dye removed by EG at equilibrium and K_f (mg/g)(L/mg)$^{1/n}$ and $1/n$ are constants representing the adsorbent capacity and the heterogeneity factor, respectively (Desta, 2013; Li et al., 2019). The plot of log q_e against log C_e determines the value of $1/n$ and K_f.

2.4. Adsorption kinetics

In the present study, kinetic models such as pseudo-first-order model, pseudo-second-order model, and diffusion-based models such as intra-particle diffusion model, and liquid film diffusion model were used to analyze the adsorption mechanism of five different dyes by EG. The kinetic models can be presented in different (linear and non-linear) forms as follow

The equation used in the linear pseudo-first-order model (LPFO) is

$$\ln(q_e - q_t) = \ln(q_e) - k_1 t \tag{4}$$

The equation used for the non-linear pseudo-first-order model (NLPFO) is

$$q_t = q_e\left(1 - e^{-k_1 t}\right) \tag{5}$$

where,$q_t$is the amount of dye adsorbed at time t (mg g^{-1}), q_e is adsorption capacity in the equilibrium (mg g^{-1}), k_1= pseudo-first-order rate constant (min^{-1}), t is the contact time (min).

Graphs of $\ln(q_e - q_t)$ versus t were plotted for five different dyes at five different dye concentrations and the slope and intercept of the obtained plot were used to determine rate constant k_1 and equilibrium adsorption capacity q_e respectively.

The equation used in the linear pseudo-second-order kinetic model (LPSO) is

$$\frac{t}{q_t} = \frac{1}{k_2 q_e^2} + \frac{1}{q_e} t \tag{6}$$

The equation used for the non-linear pseudo-second-order model (NLPSO) is

$$q_t = \frac{k_2 q_e^2 t}{1 + k_2 q_e t} \tag{7}$$

where, q_t (mg g−1), q_e (mg g−1), and t (min) are as defined in the previous equation and k_2 (g mg−1 min−1) is the pseudo-second-order rate constant (Markandeya et al., 2015; Yang and Liu, 2014; Oyelude et al., 2017). The values of q_e and k_2 were obtained by finding the slope and intercept of t/qt versus t plots.

The equation used for the intra-particle diffusion model analysis is

$$q_t = k_3 t^{1/2} + C \tag{8}$$

where q_t (mg/g) and t (min) are as previously defined, k_3 (mg/g/min$^{1/2}$) is the intraparticle diffusion rate constant and C is a constant of the boundary layer. The values of k_3 and were obtained from the slope and intercept of q_t against $t^{1/2}$ plot (Oyelude et al., 2017).

The equation used in the liquid film diffusion model is

$$-\ln(1 - F) = K_4 t + C \tag{9}$$

where F is fractional attainment of equilibrium (q_t/q_e), k_4 (1/min) is the liquid film diffusion rate constant, t (min) is time, and C is a constant related to the boundary layer. The value of k_4 was determined from the plot of –ln(1 − F) against t (Oyelude et al., 2017).

2.5. Adsorption thermodynamics

To calculate the thermodynamic parameters experiments were carried out at different temperatures in the range of 303 K to 353 K for five different dyes adsorption by EG. The effect of temperature on the adsorption kinetics of five different dyes was evaluated by calculating the dimensionless constant k_e^0.

Dimensionless equilibrium constant k_e^0 is calculated using the equation

$$k_e^0 = k_g \times \frac{C_{dye}}{\gamma} \tag{10}$$

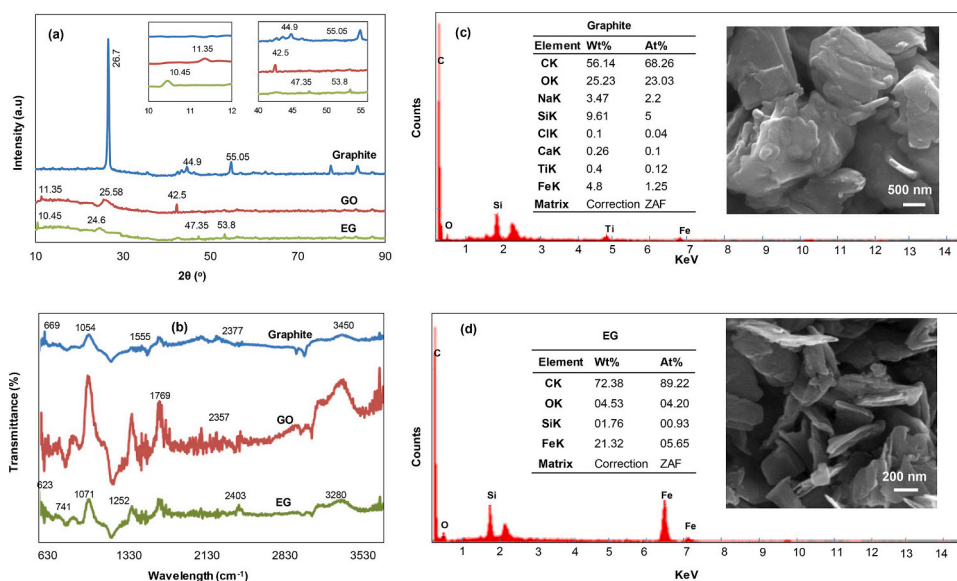Where k_g (L mol^{-1}) is the equilibrium constant of the best fit of Langmuir

Fig. 2. (a) XRD (b) FTIR (c) SEM and EDAX analysis of graphite, GO, and EG

isotherm model on experimental data, C_{dye} (mol L^{-1}) is the concentration of the adsorbate and γ is the coefficient of activity of the adsorbate. In the present study, the considered dyes' concentration was 10^{-5} mol/L and hence the value was considered as one (Lima et al., 2019; Zamri et al., 2021).

The Gibbs free energy change ($\Delta G°$) of adsorption reaction is calculated using

$$\Delta G° = -RT\ln k_e^0 \qquad (11)$$

where R is the gas constant (8.314 Jmol^{-1}K^{-1}), T is the temperature (K).

The entropy ($\Delta S°$) and enthalpy ($\Delta H°$) parameters were calculated using the equation

$$\Delta G° = \Delta H° - T\Delta S° \qquad (12)$$

where, standard enthalpy ($\Delta H°$), standard entropy ($\Delta S°$) are calculated from the above-mentioned equation by finding the intercept and slope respectively for the plot of $\Delta G°$ and T of five different dyes (Lima et al., 2019; Liu, 2009; Zamri et al., 2021).

3. Results and discussion

3.1. Preparation mechanism of EG from industrial graphite

The mechanism behind the synthesis of exfoliated graphene from graphite is an analogy to 'open a closed book to paper by paper like a paper accordion' as illustrated in Fig. 1. The oxidants and intercalants used in modified Hummer's method fused through the layers and relaxed the structural bonding in graphite (closed book), further broadened the interplanar spacing that ended up with GO (open book or paper accordion). During the thermal activation at different temperatures, the generated heat wave diffused through the macro and micro-channels of GO which relaxed the structural stability and peeled it into layers. Besides, the thermal activation sublimated the bound water molecules, O$_2$, and oxygen-containing functional groups that connected the GO layers to gas. This simultaneous depilation and reduction resulted in exfoliated graphene (paper by paper). The activation temperature of 900°C resulted in the maximum exfoliation with thin graphene layers and was so considered as the optimum activation temperature. Lower temperature (500°C-700°C) limited the exfoliation whereas higher temperature produced fragmented and melted EG. This mechanism was formulated from the characterization of obtained

products at every step that was explained in the following sections. Hence, the EG adsorbent was synthesized from GO using a thermal method which eliminated the usage of ecologically damaging chemicals and reductants and makes the method eco-safe.

3.2. Characterization

X-ray diffraction (XRD) analysis of graphite, GO and EG is a robust way to detect the micro-level structural changes during the synthesis of EG from graphite(Ammar et al., 2016; Kartick et al., 2013; Rattana et al., 2012; Wang et al., 2017). In Fig. 2(a), the peaks at 26.7°, 44.9°, and 55.05° observed can be assigned to the planes 002, 101, and 004, respectively for graphite. The sharp peak at 26.7° evidenced the crystalline nature of graphite that has an interplanar spacing of 3.34 Å. The pushing of the sharp peak from 26.7° to lower angles having a broader peak at 25.58° for GO and 24.6° for EG suggested an increased interlayer spacing and weakened π- π stacking interaction(Ammar et al., 2016; Avouris and Dimitrakopoulos, 2012; Kartick et al., 2013; Wang et al., 2017). Applying Bragg's equation, the interlayer spacing was found to be 7.79 Å and 8.45 Å for GO and EG$_{900}$ considering the 002-plane peak, proposing the intercalation, structural relaxation, and exfoliation, happened during the oxidation and thermal activation process during the synthesis process (Avouris and Dimitrakopoulos, 2012; Kartick et al., 2013). The changes observed in the interlayer spacing specify the disruption of various oxygen-containing functional groups that were bound to the graphite during its conversion to EG. The broadening and weakening of peaks during the conversion from graphite to EG confirm the presence of a few-layered reduced GO in EG (Wang et al., 2017). The rise of temperature to 900°C dries the water molecules in the GO layers during the thermal activation that may aid the exfoliation. The other peaks in the XRD spectrum may correspond to inorganic compounds which were measured in EDAX analysis. In this study, the GO synthesized from graphite was thermally reduced to EG. The thermally exfoliated EG lacks the peaks that the GO has, which illustrated that the disappearance of oxygen from the GO (Kartick et al., 2013), which was proven again in EDAX and FTIR analysis.

As shown in Fig. 2(b), the peaks at 669, 1555, 2350, and 3450 cm^{-1} wavelength in the FTIR spectra of graphite are due to the C-C bonds, C=C aromatic benzene ring including one double bond, 2 double bond, and alternate single bond, stretching vibrations of the carboxyl group (-COOH), respectively proved that the graphite is good in quality and free from any organic contaminations(Bykkam et al., 2013; Kartick
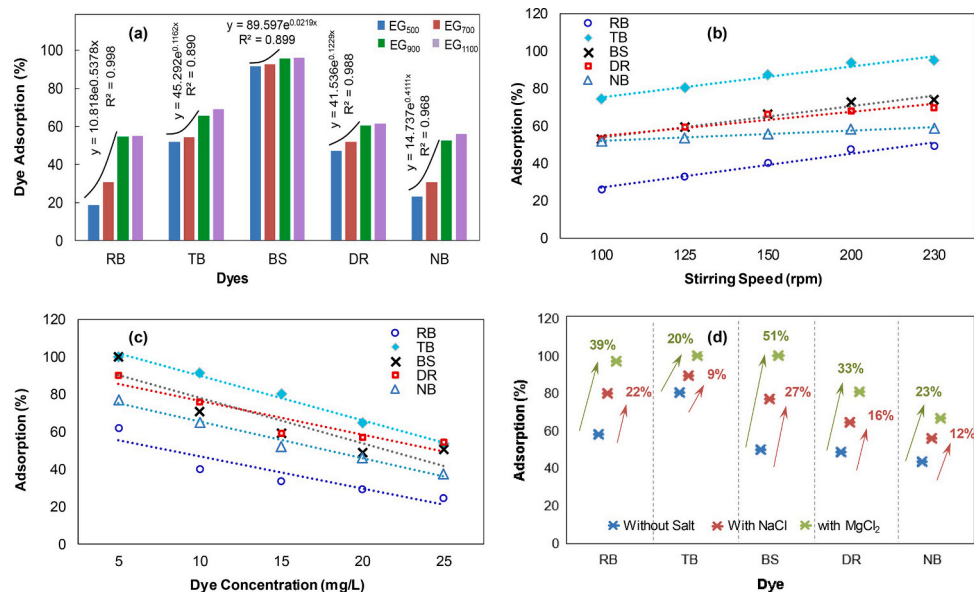
Fig. 3. Effect of (a) activation temperature (b) shaking speed (c) dye concentration (d) presence of salt on EG_{900} mediated dye adsorption

et al., 2013; Khalili, 2016; Wang et al., 2017). The firm and intense peaks at 1400-1555cm^{-1} attributes to C-OH stretching and –OH bending, 1634cm^{-1} -is due to internal alkenes, 1034 cm^{-1} indicates the vibrational mode of the C-O group, 1362 cm^{-1} is due to C-OH group, 1700 cm^{-1} is due to the presence of carboxyl group(Avouris and Dimitrakopoulos, 2012; Kartick et al., 2013; Pei et al., 2018). For GO, the resonance peak at 1634cm^{-1} can be assigned to the stretching and bending vibration of -OH groups of water molecules adsorbed on graphene oxide. The clear peaks at1750cm^{-1} characteristics to the C=O stretching vibrations of conjugated acid especially in the form of dimmer appear in GO indicating that further breakage of larger particles would create more active sites, which are prone to oxidize easily(Habte et al., 2019; Khalili, 2016).

The peaks at, 2026 –2300cm^{-1} the hydrogen-bonded OH groups of dimeric COOH groups and intra-molecular bonded O-H stretching of alcohols(Avouris and Dimitrakopoulos, 2012; Kartick et al., 2013; Pei et al., 2018), 3071, is responsible for stretching vibrations of the hydroxyl group, where the hydroxyl groups may be from absorbed water molecules, 3224 and sharp 3566cm^{-1}, –OH stretching (reveals the presence of hydroxyl groups in graphene oxide)(Bykkam et al., 2013; Ghorbani et al., 2015; Habte et al., 2019; Pei et al., 2018). In EG, the characteristic peaks of GO at 1634, 3071 cm^{-1}vanish or appear with significantly lower intensity after reduction. Blunted peaks at 1359, 1750, 2357, 3071 cm^{-1} indicate that the GO is reduced to a great extent. These bands completely disappear in the FTIR spectra of EG and the new peaks are set in1378 cm^{-1}, skeletal vibrations of graphene backbone chain and 3267 cm^{-1}, and blunted 3569 cm^{-1} OH stretching vibration (Habte et al., 2019; Kartick et al., 2013).

The BET analysis showed the surface area of 4.972 and 0.025 m^2/g and the pore volume of 0.025 and 0.102 (cm^3/g) for graphite and EG, respectively. This observation evidences the effectiveness of the chemicothermal processes involved in the conversion of graphite to EG which was further expected to assist in the performance enhancement of adsorption. Similar observations were made during the evaluation of exfoliation temperature on the characteristics of EG.

The surface morphology of the graphite and EG in Fig. 2(c and d) shows the expansion and exfoliation of few-layered graphene from initial graphite waste. The EDAX analysis showed that the industrial graphite waste has a carbon to oxygen ratio (C/O) of 2.96 whereas C/O in EG was 21.24 proved the removal of oxygen from the graphite during its conversion to EG (El-Hendawy, 2003). The disappearance of inorganic foreign matters was also evidenced.

3.3. Adsorption experiments and isotherms

3.3.1. Effect of temperature during thermal activation

To check the influence of thermal activation temperature in the adsorption capacity of EG, the performance of EG_{500}, EG_{700}, $EG_{900}$and EG_{1100} were tested for the adsorption of five different dyes, RB, TB, BS, DR, and NB. The maximum absorption wavelength of each dye was found using UV-Visible spectrum and listed in Table S1 which were matched with the datasheets of different dyes.

For all the dyes, the adsorption is positively correlated with the activation temperature and stabilized at 900°C as shown in Fig. 3(a). The EG_{900} exhibited a maximum of 96% adsorption efficiency for BS and a minimum of 53% for the dye, NB. The reason behind the stabilization of adsorption after 900°C may be the limitation of the thermal conversion of GO to EG. The possibility of melting the spiked graphene layers on the surface and further hindrance in exposing the surface of GO to the thermal activation may also end up with the equilibrium phenomenon. A distinct swift in adsorption from lower to higher temperatures (Fig. S3) was observed as shown in Fig. 3(a). The reason was found that at the low temperature of 500°C and 700°C, the exfoliation of GO is partial, and hence the surface of EG is exposed to the adsorption of dyes (Kartick et al., 2013). The thermal activation at 900°C not only favoring the exfoliation but also produces underdeveloped structures and small surface area that leads to the enhancement of structural features and adsorption capacity as shown in Fig. 2(d). This better adsorption phenomenon was witnessed with the chemical synthesis of graphene due to incomplete surface modification (Aljeboree et al., 2017). From here on, the rest of our studies were conducted only on EG_{900}.

3.3.2. Effect of shaking speed

The adsorption and adsorption rate was positively influenced by the shaking speed from 100 rpm to 250 rpm for all the dyes as shown in Fig. 3(b). With increased shaking, the rate of diffusion of dye molecules from the bulk liquid phase to the solid phase and thinning of boundary liquid layer on the surface of EG_{900} resulted in a 10% to 50% increase in adsorption for NB and RB, respectively when shaking speed changed from 100 to 200 rpm. The adsorption got stabilized at 150 rpm for DR and 200 rpm for the other dyes. Previous studies also stated the direct correlation of adsorption with shaking speed only up to a certain limit, and no correlation beyond that shaking speed (Arafat et al., 1999; Ihsanullah et al., 2015; Shiau and Pan, 2004). Turbulence-assisted agglomeration of EG_{900} particles and further hindrances of the active
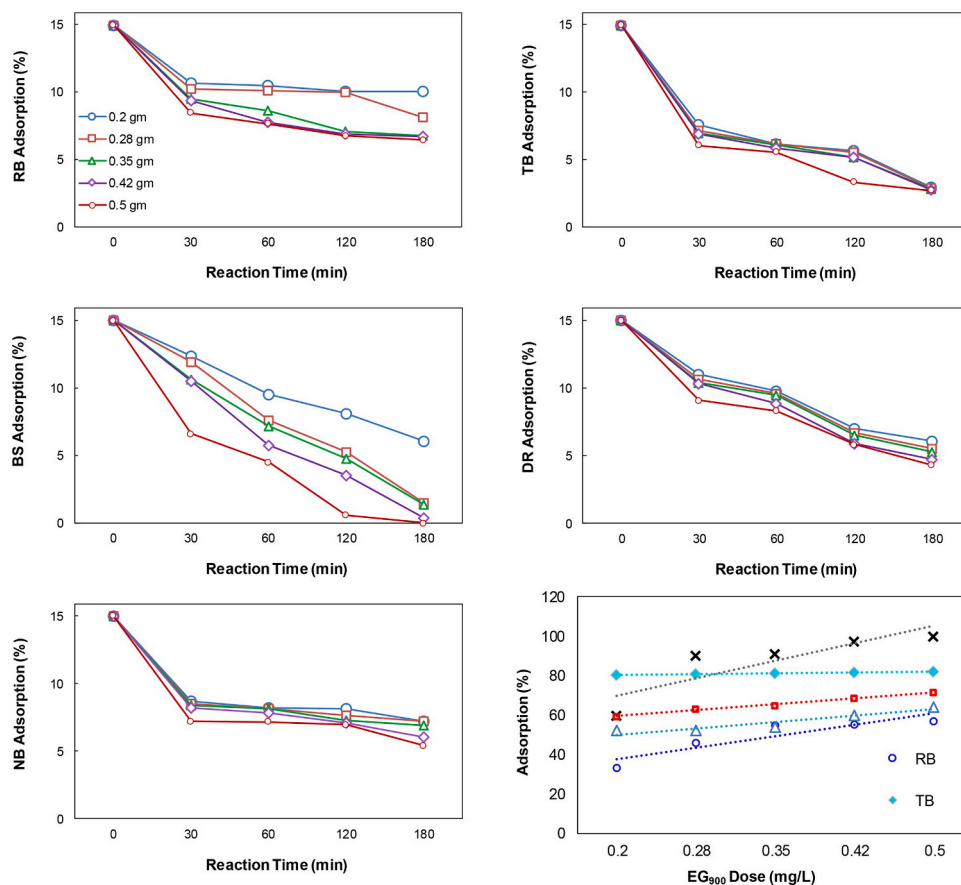
Fig. 4. Effect of EG$_{900}$ dose on dye adsorption

surface area is the reason behind this observation.

3.3.3. Effect of initial dye concentration

The influences of the initial concentration of each dye (5 to 25 mg/L) on its removal efficiency after 3h are given in Fig. 3(c). The EG$_{900}$ dose was kept as 0.2 mg/L. The dyes TB and BS showed complete removal at their initial concentration of 5ppm. Maximum dye removal occurred at low initial dye concentrations and the adsorption (%) gradually decreased towards higher concentrations, which was seen in adsorption using carbon-based adsorbents (Aljeboree et al., 2017; Nsami and Mbadcam, 2013; Priddy and Hanley, 2003); TB resulted in 100% adsorption at 5mg/L of initial concentration and halved (54%) at 25 mg/L. The adsorbent EG$_{900}$ has a fixed number of active sites which get saturated at low concentrations of the dye. Hence at higher dye concentrations, no further adsorption can be achieved, resulting in a decrease in adsorption efficiency. At 10 and 25 mg/L of dye concentration, the adsorption efficiency of EG$_{900}$ followed the order of TB > DR > BS > NB >RB and DR > TB > BS > NB > RB, respectively proved that apart from the role of dye concentration and EG900 dose, the characteristics of a dye such as its chemical structure and molecular weight also play a major role in fixing the adsorption capacity. The detailed characteristics of the dye are mentioned in the supplementary information.

3.3.4. Effect of salt

Dissolved salts in aqueous media (dye solutions) were suggested to have been involved in a variety of mechanisms which include altering the surface charge ofEG$_{900}$ and interaction with dye in both the solution and on the surface of EG$_{900}$ as witnessed with activated carbon-based adsorption (Hashemian et al., 2013).Fig. 3(d) compares the adsorption efficiency with and without salt added for a reaction time of 1h. The adsorption efficiency for each dye was found to increase with the

addition of salts NaCl and MgCl$_2$. The enhancement inefficiency was found to be in the range of 8% to 22% using NaCl and it almost doubled in the case of MgCl$_2$ and resulted in 16% to 47% for various dyes. Theoretically, when there is an electrostatic attraction between adsorbent and adsorbate an increase in ion strength shall decrease adsorption strength (Feng et al., 2011). But in the present study opposite phenomenon was observed and can be explained as follows.

As described below, when dyes were released into an aqueous solution, they got separated into negative ions and Na$^+$ ions. Upon introducing NaCl, the number of Na$^+$ ions in the solution increases and the resultant concentric cations try to neutralize the surface of EG. Meanwhile, the remaining anions were forced to aggregate and migrate towards the adsorbent surface thereby increasing the removal efficiency (Ara et al., 2015). Also, electrostatic attractions between EG and dye anions might have dominated the repulsions due to Na$^+$. The effect of Mg^{2+} mediated adsorption enhancement was greater due to its smaller hydrated radius and high atomic number. It can also be attributed due to the presence of non-electrostatic forces and dispersive interactions. These forces were enhanced with increasing ion strength which screened the electrostatic interaction and resulted in increased adsorption capacity as observed during the previous study on the adsorption of dye on magnesium hydroxide-coated pyrolytic bio-char (Zang et al., 2013).

The maximum uplift in adsorption efficiency was found with RB dye. Thus, the strength of ionic interaction between the more negative dye and the less negative EGO$_{900}$ increases, thereby enhancing adsorption efficiency (Hashemian et al., 2013).

3.3.5. Effect OF EG$_{900}$dose

The studies were conducted at 15 mg/L of each dye unless otherwise specified; the dosage of EG$_{900}$ was varied from 0.2 to 0.5 gm. Fig. 4 depicts the effect of adsorbent dose for each dye. In this experiment, the
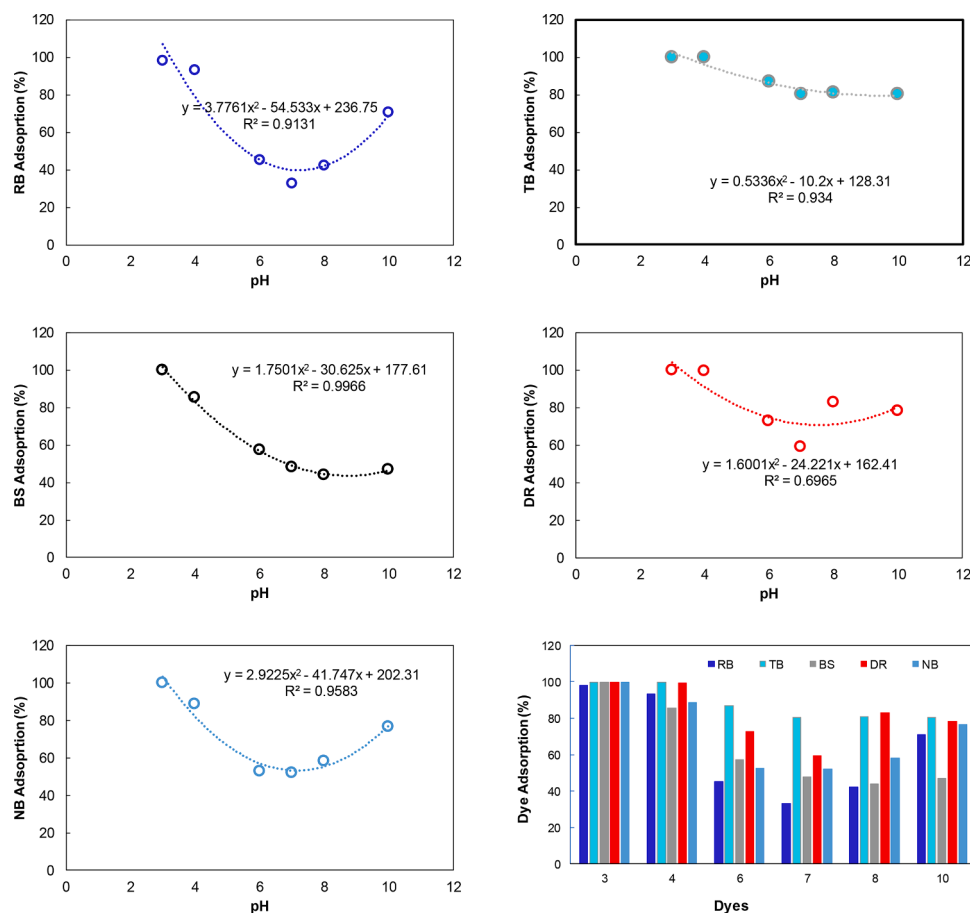
Fig. 5. Effect of pH

adsorption process is dependent on the mass of the EG_{900} which is directly proportional to the surface area of the adsorbent. From the results, it can be observed that the dosage of EG_{900} was proportional to the removal efficiency of all dyes. This can be attributed to (i) a higher concentration gradient between dye and EG, (ii) the availability of larger reactive surface areas and so a greater number of adsorptive sites, and (iii) a decrease in the adsorption density. The BS dye exhibits the highest difference in adsorption with the EG_{900} dose and attained 100% removal efficiency at 0.5 gm in 3 h adsorption time. However, for the other dyes, the increase in adsorption capacity was weakened as more EG_{900} is used, because of the incomplete utilization of the full capacity of EG_{900} and fixed dye concentration. This fact also may be due to the agglomeration effect of EG_{900} that tends to occur at higher dosages and the hindrance of active sites on EG_{900}. Besides, the increase in adsorption efficiency observed is non-linear for BS and tends to attain a stable value at a higher dose and hence resulted in a low R^2 value as observed before in adsorption studies using activated carbon derived from coconut shell and cola nutshell(Nsami and Mbadcam, 2013; Priddy and Hanley, 2003). The concentration of dye during stabilization followed that order BS > TB > DR > NB > RB, as given in Fig. S4.

3.3.6. Effect of pH

The adsorption phenomenon depends on the structure and solubility of the dye, and the charge of the adsorbent, EG_{900}'s surface which was controlled by the pH of a dye solution, as any change in the pH can affect the three major influencing factors of adsorption and hence the ionic interaction between the dye and EG_{900} (Hu et al., 2019; Shittu et al., 2019; Sykam et al., 2018; Yusuf et al., 2015). The results obtained as illustrated in Fig. 5 showed that the general trend of obtaining maximum adsorption efficiency at pH 3 with 98 to 99.9% removal of dyes and

weakening of adsorption towards circum-neutral pH and a rising at alkaline pH conditions (Zhu et al., 2010). The least adsorption was found to be at pH 7 for RB, TB, DR, and NB and 8 for BS. However, for all the dyes an increase in adsorption efficiency was observed at alkaline pH and reached 46% of adsorption with BS and 70% to 81% with other dyes, and the uplift was found to be the least of 0.9% with TB.

To catch on the reason, the zeta potential of EG_{900} was analyzed. It was found to be negative in the range of -89.24 to -109.94 mV for all pH conditions, which may be due to the structural defects and functional groups such as -COOH, C=O which would facilitate the adsorption (Shittu et al., 2019). The dyes used for the study have a complex organic structure with unsaturated bonds having -SO_3Na as the functional group. The pKa values of different attractor groups representing the dye molecule, sulfonic acid group (SO_3^-), carboxylate group (COO^-), and azo group (N = N) were 2.0, 5.0, and 10.86, respectively. If pH of solution > pKa of the dye, the dye molecules exist in anionic form. For instance, the pKa of the sulphonic group is 2, and if the pH of the solution is 3-10 which means the surrounding environment is basic and hence sulphonic group exists in de-protonated form (Zhu et al., 2010), and resulted in anionic species as shown in the following Eq. (10).

$$Dye - SO_3Na \rightarrow Dye - SO_3^- + Na^+ \qquad (10)$$

Meanwhile, when H^+ ions were added to lower the pH, there is a simultaneous gain in positive surface charge and reduction in negative surface charge due to the uptake of H^+ ions by the surface of EG_{900} and enhanced the adsorption of anionic dye species (Zhu et al., 2010). With the increment in solution pH towards circum-neutral pH, the competition between OH^- ions and the anionic dye species in interacting with the surface of EG_{900} results in minimum adsorption efficiency. The rise in adsorption at alkaline pH can be attributed due to the small formation of

Table 1
Langmuir and Freundlich isotherms

Dyes	Langmuir				Freundlich		Best Fit
	K_L (L/mg)	q_{max} (mg/gm)	R^2	K_f	1/n	R^2	Model
RB	0.274	36.231	0.981	12.377	0.31	0.975	Langmuir
TB	3.769	68.027	0.998	36.693	0.28	0.617	Langmuir
BS	0.766	60.975	0.929	1.233	0.332	0.959	Freundlich
DR	0.46	74.074	0.925	28.131	0.327	0.962	Freundlich
NB	0.442	54.054	0.996	19.443	0.347	0.971	Langmuir

coagulated molecules and precipitation of dye color at basic pH. The synergistic effect of competition between anions and the no-coagulation effect is the fact behind the least adsorption at circum-neutral pH conditions. Even then hydrogen bonding and hydrophobic mechanisms are inclusive, the main mechanism was found to be an electrostatic

attraction between the dyes and the adsorbent, EG$_{900}$. This trend holds good for all the dyes studied.

3.3.7. Adsorption isotherms and adsorption capacity

After equilibrium is reached, adsorption isotherms are useful to understand the liquid phase dye molecule, which is adsorbed on the solid phase adsorbent, EGO$_{900}$. Both Langmuir and Freundlich isotherms were plotted for all the dyes as shown in Fig. S5 to express the adsorption of different dyes by EGO$_{900}$ at the equilibrium time of 3 h at a constant temperature, 298 K, and the calculated isotherms constants were listed in Table 1. By comparing the R^2 charts for each dye, the isotherm model which it followed was predicted as described in the literature (Oyelude et al., 2017).

The 'closer to unity' R^2 values for the dyes, RB, TB, and NB indicating these dyes follow the Langmuir model that assumes the homogenous monolayer adsorption occurring on a surface of EG$_{900}$ which contains sorption sites having uniform binding energy. Hence, no adsorption
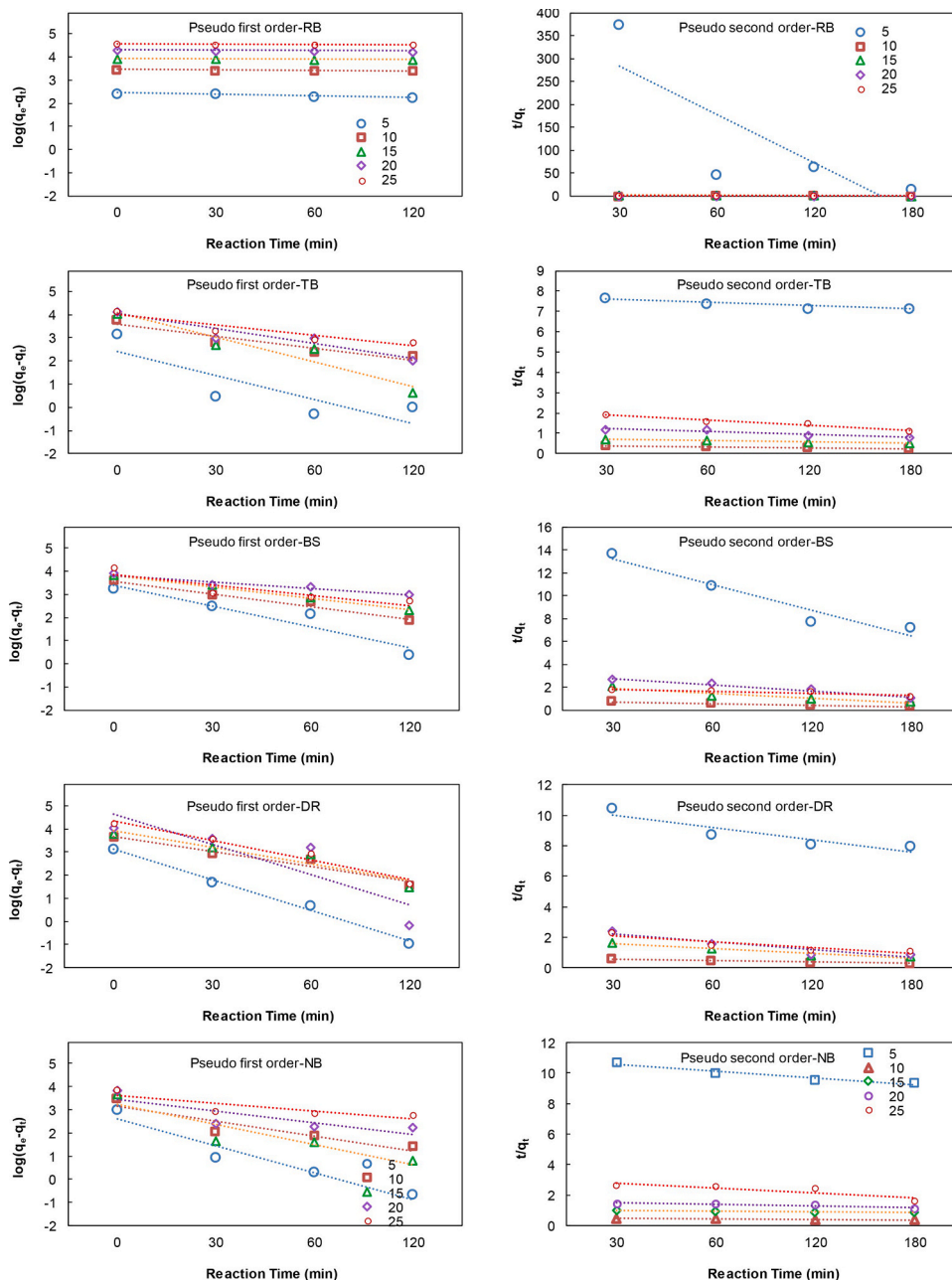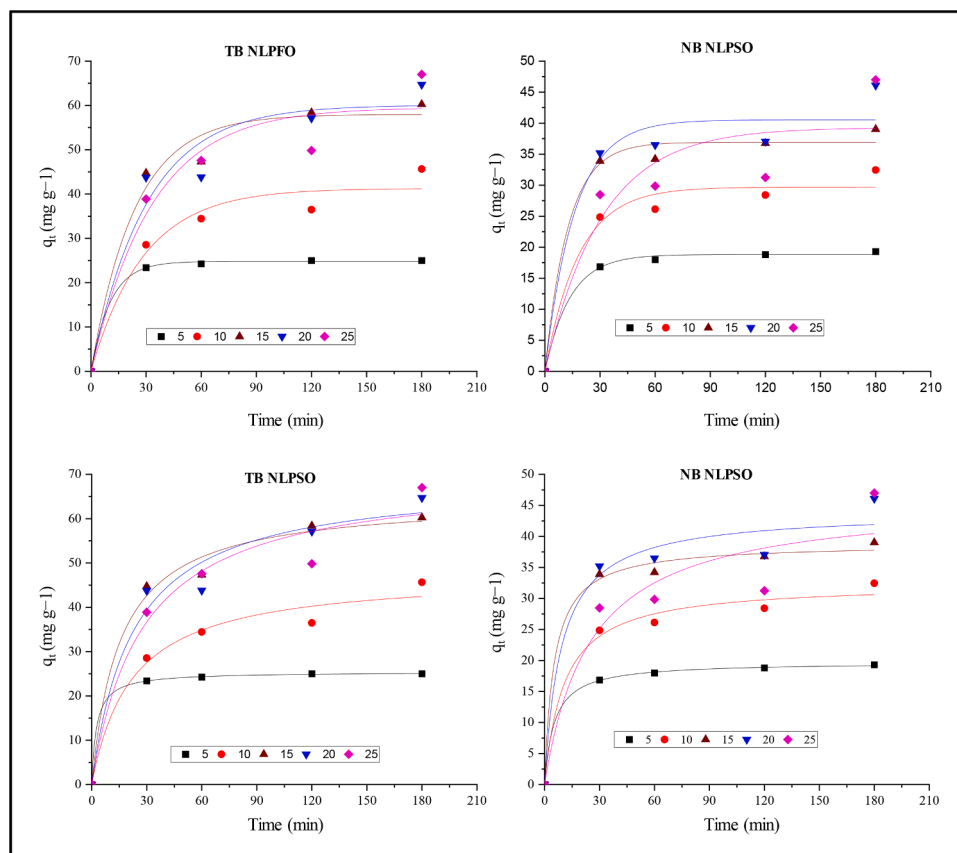

Fig. 6. Pseudo-first and second-order kinetics

Fig. 7. Non-Linear-Pseudo-First Order and Pseudo-Second Order Models

occurs when RB, TB, and NB adsorbate molecules fill these sites on EG$_{900}$. The maximum adsorption capacity calculated was 36.23, 68.02, and 54.05 mg/gm for the dyes RB, TB, and NB which almost matched with the experimental observation also 30.805, 67, and 47 mg/L, respectively.

Freundlich isotherm was also plotted to check to see if it's a better fit. For the dyes BS and DR, the Freundlich isotherm was a better fit and it showed that the adsorption capacity of 57.974 and 62.245 mg/gm for the dyes BS and DR, respectively for which the experimental observation was 63.173 and 68.28 mg/gm. At this point, the fact is Freundlich isotherm assumes multilayer adsorption with the heterogeneous surface where binding sites on EG$_{900}$ are not equivalent. Identical information was detailed in teak leaf little powder-based adsorption of eosin yellow dye (Yang and Liu, 2014). The 1/n values obtained from the Freundlich isotherm were less than 1 for all dyes indicate normal adsorption and the partition between the solid phase EG$_{900}$ and liquid phase dyes depends on concentration. However, the validity of these assumptions based on the isotherm fit cannot be concluded as, in a solution-solid adsorption system because various factors like hydration forces and mass transport effects, and concentration play a role, making the whole system is dynamic and complicated. Therefore, obeying the isotherms does not mean that the assumptions are valid. In such systems the isotherm adequacy can be seriously affected by the experimental conditions, in particular, the range of concentration of the solute, dyes, and dose of adsorbate, EG$_{900}$.

The prepared EG$_{900}$ showed the adsorption capacity which is almost equal to the existing well-used adsorbent, activated carbon (Fig. S6), and can be the best alternate for activated carbon which demands huge carbon and water footprint for its preparation.

3.3.8. Adsorption kinetics

Adsorption kinetic study plays an important role in understanding

the mechanism of the adsorption process and the rate-controlling step (Oyelude et al., 2017; Yang and Liu, 2014). It provides valuable information regarding the dynamics of the adsorption process in terms of rate constant and order that can play an important role in designing and modeling the actual treatment system(Yang and Liu, 2014). In the present study (linear and non-linear) forms of pseudo-first and second-order kinetics, intra-particle diffusion, and liquid film diffusion models were tested to understand the adsorption of dyes by EG$_{900}$.

3.3.8.1. Pseudo first and second-order kinetics. Based on the adsorption equilibrium capacity, the adsorption of dyes by EG$_{900}$was described by linearized pseudo-first and second-order models as in Fig. 6. The closeness of q$_e$ calculated values to the q$_e$ experimental values was observed for RB, BS, and DR dyes. It proves that the linearized pseudo-first-order model is the best fit model to describe the kinetics of their removal from aqueous solution by EG$_{900}$ (Oyelude et al., 2017). Besides, it was observed that the linearized pseudo-first-order determination coefficient (R^2) values are higher than those of linear pseudo-second-order values (Table S2(a-b)) which proves that for the above-mentioned three dyes linear pseudo-first-order kinetic model is the best fit model. Hence it can be concluded that the rate of dye adsorption is proportional to the number of free adsorption sites (Amadi et al., 2017).

For TB dye and NB dye variation in q$_e$ calculated (q$_e$ cal) to the q$_e$ experimental (q$_e$ exp) values were observed with lesser R^2 values. It indicates that the linearized form of pseudo-first and second-order models didn't fit well to describe the adsorption kinetics. However, the chances of non-linearized forms of first and second-order kinetic models of describing them cannot be ignored (Markandeya et al., 2015). Hence, the adsorption of TB and NB dyes was described by its NLPFO and NLPSO models as shown in Fig. 7. From Table S2(b and d), it can be observed that q$_e$ cal values are increasing with the increase in the dye
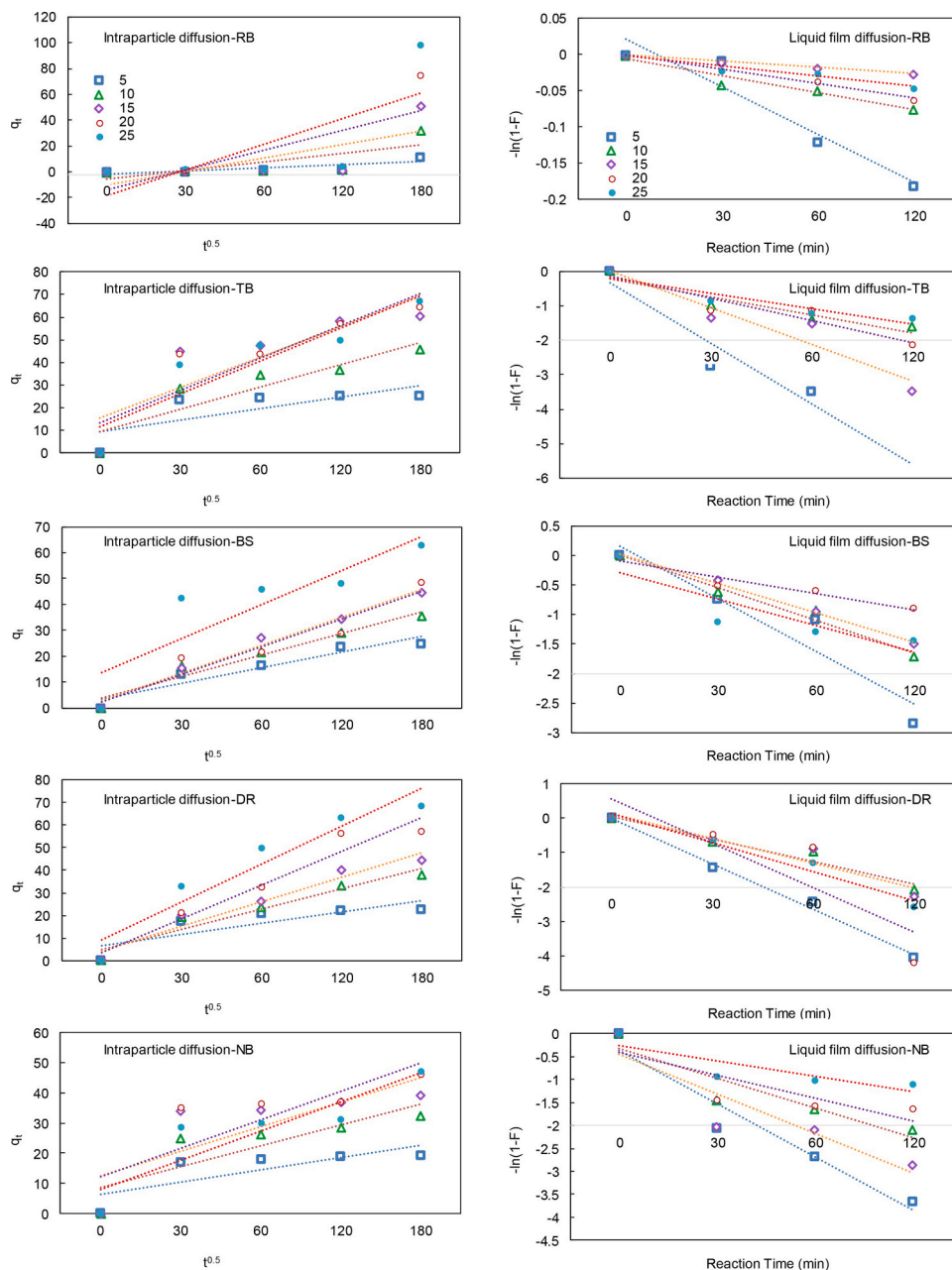
Fig. 8. Intraparticle and liquid-film diffusion Model

concentration following the similar path of q_e exp. More closeness of q_e cal values to q_e exp can be observed in the NLPSO model than in NLPFO for both the dyes. Also, the determination coefficient (R^2) values are observed to be higher for PNLSO than NLPFO. Based on the above two criteria it can be clearly stated that NLPSO kinetic model was found to be the best fit model for TB and NB dyes to describe their adsorption kinetics by EG_{900} (Markandeya et al., 2015).

3.3.8.2. Intra particle diffusion. The plots of q_t vs $t^{1/2}$ of five different dyes are shown in Fig. 8. The value of C, R^2, and second-order rate constant (K_3) for 0.2 g EG adsorbent dose at five different dye concentrations for five different dyes are calculated and listed in Table S2(c). As adsorbed dye molecules can move from the surface of EG_{900} into the pores, this diffusion model plays an important role in evaluating the influence of pore diffusion on the adsorption mechanism (Oyelude et al., 2017). It was observed from Fig. 7 that the plots are linear but not passing through the origin and have non-zero intercepts. It concluded

that intra-particle diffusion was involved in the current adsorption process, however not the sole rate-limiting step (Yang and Liu, 2014; Pan et al., 2017).

3.3.8.3. Liquid film diffusion. The plots of $-\ln(1 - F)$ vs t of five different dyes are linear and are close to passing the origin as shown in Fig. 8. A similar result was also found by Yang et al. 2015 which states that liquid film diffusion cannot be exempted from the adsorption process and adsorption kinetics is likely to be diffusion-limited. Also, Table S2(d-e) shows that the value of liquid film diffusion rate constant (k_4) is less than the intra-particle diffusion rate constant (k_3) for all dyes which indicates that the liquid diffusion process can be the rate-limiting step (Yang and Liu, 2014; Tarawou and Young, 2015).

As the linear plots of the intra-particle and liquid film diffusion didn't pass through the origin which can also indicate that boundary layer diffusion might have involved in the adsorption process and both liquid film diffusion and intra-particle diffusion can jointly control the

removal of dyes from aqueous solution by EG$_{900}$ (Oyelude et al., 2017).

3.3.9. Thermodynamic parameters

The Gibbs free energy changes (ΔG°) for the adsorption of five different dyes onto EG were calculated using the eq. (8) whereas ΔS° and ΔH° parameters are calculated by finding slope and intercept of ΔG° vs T plots as shown in Fig. (S5), at different temperatures for five different dyes. All the thermodynamic parameters at different temperatures are summarized in Table S3.

It was observed that ΔG° value for all dyes is negative which means the adsorption process is spontaneous and is more favorable in the temperature range of 303 to 353 K. It can also be observed that ΔG° increased on increasing the temperature from 303K to 353K which shows that process is not favorable at high temperatures for all five (Lyubchik et al., 2020).

The ΔH° values are 2.738, 2.746, 2.734, 2.715, 2.771 KJ/mol for RB, TB, BS, DR, and NB dyes, respectively. As all ΔH° values are positive, the adsorption process is endothermic. According to Svetlana et al., 2014, the heat evolved in the range of 2.1-20.9 kJ/mol undergoes physical adsorption, 80-200 kJ/mol enthalpy change is chemisorption, and <8.4 kJ/mol enthalpy changes were observed for ion exchange reactions. In the present study, the enthalpy value for all the dyes is< 20 kJ/mol which shows it is physical adsorption. Similarly, the ΔS^0 value was found to be 0.110, 0.135, 0.121, 0.112, and 0.114 KJ/mol for RB, TB, BS, DR, and NB dyes respectively. The positive ΔS^0 indicates the increased randomness at the solid and liquid interface (Pan et al., 2017) (Lyubchik et al., 2020). Overall, it shows physical adsorption with increased randomness for all five dyes.

4. Conclusion

This study successfully converted the industrial graphite waste to a beneficial material viz exfoliated graphite (EG) by an eco-safe chemicothermal process. The resultant EG was micro-analyzed to exhibit favorable characteristics towards adsorption. Subsequently, the adsorption efficiency of EG was checked against the removal of five toxic dyes, which are used as fabric colors in textile industries. The efficacious and complete adsorption of toxic dyes that were observed in this study, suggests extending the application of EG to remove complex organic pollutants in pharmaceutical, food products, and oil manufacturing industrial effluents. The conversion of massive industrial graphite waste to the engineeredadsorbent and its capability of replacing the currently practiced activated carbon which claims huge water and carbon footprint are the major milestones that were achieved in this study, in the area of waste to wealth. Also, the results of the industrial graphite waste-derived, EG-mediated removal of toxic dyes proved an operational example of circular economy aspects in a real-world industrial scenario. The coupling of beneficial industrial graphite waste management and industrial wastewater treatment with decoupling of resource consumption for the activated carbon production, not only reduces industry's impact on the local environment but also overcomes the challenges towards the greener practices in industries, and provides industries the best opportunity to achieve the sustainable development.

Declaration of Competing Interest

The authors declare that they have no known competing financial interests or personal relationships that could have appeared to influence the work reported in this paper.

Funding

Statement of novelty

The current work is the first of its kind to successfully convert auto-forge industrial graphite waste to exfoliated graphene (EG) by an eco-safe chemicothermal approach. Another novelty involves in this study is the evaluation of industrial graphite waste-derived exfoliated graphene as the engineered adsorbent for textile dyes. The study assessed the effect of varying environmental conditions such as solution pH, dye and EG dose, shaking speed, and presence of salt adsorption on the adsorption efficiency, and adsorption mechanisms were derived. Langmuir and Freundlich isotherms were drawn to understand the details of the adsorption process. The kinetic and thermodynamic models were studied to explore the mechanisms.

The synthesized EG's adsorption capacity was compared with the present-in-use activated carbon which demands huge water and carbon footprint and this study's results suggest that the prepared EG can be the top substitute for it. The above-mentioned observations and research outcome of the industrial graphite waste-derived EG and its application as textile dye adsorbent, pave a new path in the advanced research areas such as sustainable industrial waste management, waste to wealth, circular economy, and green engineering practices.

Supplementary materials

Supplementary material associated with this article can be found, in the online version, at doi:10.1016/j.envadv.2021.100072.

References

Akamatsu, K., 1962. A historical pattern of economic growth in developing countries. https://doi.org/10.1111/j.1746-1049.1962.tb01020.x.

Aljeboree, A.M., Alshirifi, A.N., Alkaim, A.F., 2017. Kinetics and equilibrium study for the adsorption of textile dyes on coconut shell activated carbon. Arab. J. Chem. 10, S3381–S3393. https://doi.org/10.1016/j.arabjc.2014.01.020.

Allen, D.T., Behmanesh, N., 1994. Waste as raw materials. The Greening of Industrial Ecosystems. National Academy press. https://doi.org/10.17226/2129.

Amadi, O.K., Odidiozor, C.J., Okoro, I.A., Okoro, O.K., Odidiozor, C.J., Kinetic, I.A.O.S., Diffusivities, I., 2017. Sorption Kinetic and Intraparticle Diffusivities of As 3 + and Hg 2 + Detoxification from Aqueous Solution Using Cellulosic Biosorbent Derived from Okra (Abelmoschus esculentus) Stems To cite this version : HAL Id : hal-01648442 Sorption Kinetic and Int. Int. J. Eng. Inf. Syst. 1, 72–85.

Ammar, A., Al-Enizi, A.M., AlMaadeed, M.A.A., Karim, A., 2016. Influence of graphene oxide on mechanical, morphological, barrier, and electrical properties of polymer membranes. Arab. J. Chem. 9, 274–286. https://doi.org/10.1016/j.arabjc.2015.07.006.

Ara, N.J., Rahman, M.J., Alam, M.S., 2015. Effect of salts on the removal of remazol Yellow by using activated charcoal prepared from sawdust. Bangladesh J. Sci. Ind. Res. 50 (4), 285–292.

Arafat, H.A., Franz, M., Pinto, N.G., 1999. Effect of salt on the mechanism of adsorption of aromatics on activated carbon. Langmuir 15, 5997–6003. https://doi.org/10.1021/la9813331.

Avouris, P., Dimitrakopoulos, C., 2012. Graphene: Synthesis and applications. Mater. Today 15, 86–97. https://doi.org/10.1016/S1369-7021(12)70044-5.

Azapagic, A., 2004. Developing a framework for sustainable development indicators for the mining and minerals industry. J. Clean. Prod. 12, 639–662. https://doi.org/10.1016/S0959-6526(03)00075-1.

Bendikiene, R., Ciuplys, A., Kavaliauskiene, L., 2019. Circular economy practice: From industrial metal waste to production of high wear resistant coatings. J. Clean. Prod. 229, 1225–1232. https://doi.org/10.1016/j.jclepro.2019.05.068.

Bruvoll, A., Ibenholt, K., 1997. Future waste generation: Forecasts on the basis of a macroeconomic model. Resour. Conserv. Recycl. 19, 137–149. https://doi.org/10.1016/S0921-3449(96)01189-5.

Bykkam, S., K., V.R., CH., S.C., Thunugunta, T., 2013. Synthesis and characterization of graphene oxide and its antimicrobial activity against Klebsiella and Staphylococus. Int. J. Adv. Biotechnol. 4, 142–146.

Capone, M., Cherubini, N., Cozzella, M.L., Dodaro, A., Guarcini, T., 2019. The exfoliation of irradiated nuclear graphite by treatment with organic solvent: A proposal for its recycling. Nucl. Eng. Technol. 51, 1037–1040. https://doi.org/10.1016/j.net.2019.01.003.

Carmen, Z., Daniel, S., 2012. Textile Organic Dyes – Characteristics, Polluting Effects and Separation/Elimination Procedures from Industrial Effluents – A Critical Overview.

Org. Pollut. Ten Years After Stock. Conv. - Environ. Anal. Updat. https://doi.org/10.5772/32373.

Chen, W., Yan, L., Bangal, P.R., 2010. Preparation of graphene by the rapid and mild thermal reduction of graphene oxide induced by microwaves. Carbon N. Y. 48, 1146–1152. https://doi.org/10.1016/j.carbon.2009.11.037.

Chung, H.K., Kim, W.H., Park, J., Cho, J., Jeong, T.Y., Park, P.K., 2015. Application of Langmuir and Freundlich isotherms to predict adsorbate removal efficiency or required amount of adsorbent. J. Ind. Eng. Chem. 28, 241–246. https://doi.org/10.1016/j.jiec.2015.02.021.

Clarke, E.A., Anliker, R., 1980. Organic Dyes and Pigments. Handb. Environ. Chem. 3, 181–215. https://doi.org/10.1007/978-3-540-38522-6_7.

Dao, T.D., Jeong, H.M., 2015. Graphene prepared by thermal reduction-exfoliation of graphite oxide: Effect of raw graphite particle size on the properties of graphite oxide and graphene. Mater. Res. Bull. 70, 651–657. https://doi.org/10.1016/j.materresbull.2015.05.038.

Dauvergne, P., Lister, J., 2012. Big brand sustainability: Governance prospects and environmental limits. Glob. Environ. Chang. 22, 36–45. https://doi.org/10.1016/j.gloenvcha.2011.10.007.

Dean, T.A., 2000. Precision forging. Proc. Inst. Mech. Eng. Part C J. Mech. Eng. 214, 113–126. https://doi.org/10.1243/0954406001522859.

Desta, M.B., 2013. Batch Sorption Experiments: Langmuir and Freundlich Isotherm Studies for the Adsorption of Textile Metal Ions onto Teff Straw (Eragrostis tef) Agricultural Waste. J. Thermodyn. 61 https://doi.org/10.1155/2013/375830 https://doi.org/dx.doi.org/.

Duan, X., Deng, J., Wang, X., Guo, J., Liu, P., 2016. Manufacturing conductive polyaniline/graphite nanocomposites with spent battery powder (SBP) for energy storage: A potential approach for sustainable waste management. J. Hazard. Mater. 312, 319–328. https://doi.org/10.1016/j.jhazmat.2016.03.009.

El-Hendawy, A.N.A., 2003. Influence of HNO3 oxidation on the structure and adsorptive properties of corncob-based activated carbon. Carbon N. Y. 41, 713–722. https://doi.org/10.1016/S0008-6223(03)00029-0.

Fellner, J., Lederer, J., Scharff, C., Laner, D., 2017. Present Potentials and Limitations of a Circular Economy with Respect to Primary Raw Material Demand. J. Ind. Ecol. 21, 494–496. https://doi.org/10.1111/jiec.12582.

Feng, Y., Yang, F., Wang, Y., Ma, L., Wu, Y., Kerr, P., Yang, L., 2011. Basic Dye adsorption onto an agro-based material- Sesame hull (Sesamum Indicum L). Bioresour. Technol. 102, 10280–10285. https://doi.org/10.1016/j.biortech.2011.08.090.

Feytis, A., 2010. The bright side of graphite 31–39.

Gao, X., Jang, J., Nagase, S., 2010. Hydrazine and thermal reduction of graphene oxide: Reaction mechanisms, product structures, and reaction design. J. Phys. Chem. C 114, 832–842. https://doi.org/10.1021/jp909284g.

Ghorbani, M., Abdizadeh, H., Golobostanfard, M.R., 2015. Reduction of Graphene Oxide via Modified Hydrothermal Method. Procedia Mater. Sci. 11, 326–330. https://doi.org/10.1016/j.mspro.2015.11.104.

Gray, R., Jan Bebbington, 2001. Accounting for the Environment.

Habte, A.T., Ayele, D.W., Hu, M., 2019. Synthesis and Characterization of Reduced Graphene Oxide (rGO) Started from Graphene Oxide (GO) Using the Tour Method with Different Parameters. Adv. Mater. Sci. Eng. 2019 https://doi.org/10.1155/2019/5058163.

Hashemian, S., Ardakani, M.K., Salehifar, H., 2013. Kinetics and Thermodynamics of Adsorption Methylene Blue onto Tea Waste/CuFe$<$sub$>$2$<$/sub$>$O$<$sub$>$4$<$/sub$>$ Composite. Am. J. Anal. Chem. 04, 1–7. https://doi.org/10.4236/ajac.2013.47a001.

Hossain, L., Sarker, S.K., Khan, M.S., 2018. Evaluation of present and future wastewater impacts of textile dyeing industries in Bangladesh. Environ. Dev. 26, 23–33. https://doi.org/10.1016/j.envdev.2018.03.005.

Hou, Y., Lv, S., Liu, L., Liu, X., 2020. High-quality preparation of graphene oxide via the Hummers' method: Understanding the roles of the intercalator, oxidant, and graphite particle size. Ceram. Int. 46, 2392–2402. https://doi.org/10.1016/j.ceramint.2019.09.231.

Hu, Z., Cai, L., Liang, J., Guo, X., Li, W., Huang, Z., 2019. Green synthesis of expanded graphite/layered double hydroxides nanocomposites and their application in adsorption removal of Cr(VI) from aqueous solution. J. Clean. Prod. 209, 1216–1227. https://doi.org/10.1016/j.jclepro.2018.10.295.

Ihsanullah, Asmaly, H.A., Saleh, T.A., Laoui, T., Gupta, V.K., Atieh, M.A., 2015. Enhanced adsorption of phenols from liquids by aluminum oxide/carbon nanotubes: Comprehensive study from synthesis to surface properties. J. Mol. Liq. 206, 176–182. https://doi.org/10.1016/j.molliq.2015.02.028.

Kalyoncu, R.S., Taylor, H.A., 2002. Natural graphite. Kirk-Othmer Encycl. Chem. Technol. https://doi.org/10.1002/0471238961.1401202120012512.a01.pub2 https://doi.org/https://doi.org/.

Kang, P., Zhang, H., Duan, H., 2020. Characterizing the implications of waste dumping surrounding the Yangtze River economic belt in China. J. Hazard. Mater. 383, 121207 https://doi.org/10.1016/j.jhazmat.2019.121207.

Kaniyoor, A., Ramaprabhu, S., 2011. Thermally exfoliated graphene based counter electrode for low cost dye sensitized solar cells. J. Appl. Phys. 109 https://doi.org/10.1063/1.3600231.

Kartick, B., Srivastava, S.K., Srivastava, I., 2013. Green synthesis of graphene. J. Nanosci. Nanotechnol. 13, 4320–4324. https://doi.org/10.1166/jnn.2013.7461.

Khalili, D., 2016. Graphene oxide: A promising carbocatalyst for the regioselective thiocyanation of aromatic amines, phenols, anisols and enolizable ketones by hydrogen peroxide/KSCN in water. New J. Chem. 40, 2547–2553. https://doi.org/10.1039/c5nj02314a.

Kryachek, V.M., 2004. Friction composites: Traditions and new solutions (review). I. Powder materials. Powder Metall. Met. Ceram. 43, 581–592. https://doi.org/10.1007/s11106-005-0025-2.

Langdon, K.A., Chandra, A., Bowles, K., Symons, A., Pablo, F., Osborne, K., 2019. A preliminary ecological and human health risk assessment for organic contaminants in composted municipal solid waste generated in New South Wales. Australia. Waste Manag. 100, 199–207. https://doi.org/10.1016/j.wasman.2019.09.001.

Larciprete, R., Fabris, S., Sun, T., Lacovig, P., Baraldi, A., Lizzit, S., 2011. Dual path mechanism in the thermal reduction of graphene oxide. J. Am. Chem. Soc. 133, 17315–17321. https://doi.org/10.1021/ja205168x.

Lavin-Lopez, M.P., Patón-Carrero, A., Muñoz-Garcia, N., Enguilo, V., Valverde, J.L., Romero, A., 2019. The influence of graphite particle size on the synthesis of graphene-based materials and their adsorption capacity. Colloids Surfaces A Physicochem. Eng. Asp. 582, 123935 https://doi.org/10.1016/j.colsurfa.2019.123935.

Lee, W.E., Zhang, S., 1999. Melt corrosion of oxide and oxide-carbon refractories. Int. Mater. Rev. 44, 77–104. https://doi.org/10.1179/095066099101528234.

Li, C., Si, X., Cao, J., Qi, J., Dong, Z., Feng, J., 2019. Residual stress distribution as a function of depth in graphite/copper brazing joints via X-ray diffraction. J. Mater. Sci. Technol. 35, 2470–2476. https://doi.org/10.1016/j.jmst.2019.07.023.

Li, K., Rimmer, S.M., Liu, Q., 2018. Geochemical and petrographic analysis of graphitized coals from Central Hunan, China. Int. J. Coal Geol. 195, 267–279. https://doi.org/10.1016/j.coal.2018.06.009.

Lima, E.C., Bandegharaei, A.H., Pirajan, J.C., Anastopolous, I., 2019. A Critical Review of the estimation of the thermodynamic parameters on the adsorption equilibria. Wrong use of equilibrium constaant in the Vant Hoff's equation for calculation of thermodynamic parameters of adsorption. J. Mol. Liq. 273, 425–434. https://doi.org/10.1016/j.molliq.2018.10.048.

Liu, Y., 2009. Is the Free Energy Change of Adorption Correctly Calculated? J. Chem. Eng. Data 54, 1981–1985.

Luo, L.jun, Li, J., Dai, J., Xia, L., Barrow, C.J., Wang, H., Jegatheesan, J., Yang, M., 2017. Bisphenol A removal on TiO2–MoS2–reduced graphene oxide composite by adsorption and photocatalysis. Process Saf. Environ. Prot. 112, 274–279. https://doi.org/10.1016/j.psep.2017.04.032.

Lyubchik, S., Lyubchik, A., Lygina, O., Fonseca, S.L., I., 2020. Comparison of the Thermodynamic Parameters Estimation for the Adsorption Process of the Metals from Liquid Phase on Activated Carbons. Intechopen 1–15.

Markandeya, Shukla, S.P., Kisku, G.C., 2015. Linear and non-linear kinetic modeling for adsorption of disperse dye in batch process. Res. J. Environ. Toxicol. 9, 320–331. https://doi.org/10.3923/rjet.2015.320.331.

Mitchell, C.J., 1992. Industrial Minerals Laboratory Manual: Flake Graphite. Br. Geol. Surv. 20, 21–33. https://doi.org/10.1108/ss.2002.11020aab.002.

Nsami, J.N., Mbadcam, J.K., 2013. The Adsorption Efficiency of Chemically Prepared Activated Carbon from Cola Nut Shells by ZnCl 2 on Methylene Blue. J. Chem. 2013, 1–7.

Oyelude, E.O., Awudza, J.A.M., Twumasi, S.K., 2017. Equilibrium, Kinetic and Thermodynamic Study of Removal of Eosin Yellow from Aqueous Solution Using Teak Leaf Litter Powder. Sci. Rep. 7, 1–10. https://doi.org/10.1038/s41598-017-12424-1.

Pan, M., Lin, X., Xie, J., Huang, X., 2017. Kinetic, equilibrium and thermodynamic studies for phosphate adsorption on aluminum hydroxide modified palygorskite nano-composites. RSC Adv. 7, 4492–4500. https://doi.org/10.1039/C6RA26802A.

Pappu, A., Saxena, M., Asolekar, S.R., 2007. Solid wastes generation in India and their recycling potential in building materials. Build. Environ. 42, 2311–2320. https://doi.org/10.1016/j.buildenv.2006.04.015.

Patterson, J.W., Cheng, M.H., 1975. Steel Industry Wastes Author (s): J. W. Patterson and M. H. Cheng Literature Review (Jun ., 1975). Steel Industry Wastes 47, 1473–1476. https://www.jstor.org/stable/25038870.

Pei, S., Wei, Q., Huang, K., Cheng, H.M., Ren, W., 2018. Green synthesis of graphene oxide by seconds timescale water electrolytic oxidation. Nat. Commun. 9, 1–9. https://doi.org/10.1038/s41467-017-02479-z.

Polprasert, C., Liyanage, L.R.J., 1996. Hazardous waste generation and processing. Resour. Conserv. Recycl. 16, 213–226. https://doi.org/10.1016/0921-3449(95)00058-5.

Pozzetto, S., Capone, M., Cherubini, N., Cozzella, M.L., Dodaro, A., Guidi, G., 2020. Proposal of a prototype plant based on the exfoliation process for the treatment of irradiated graphite. Nucl. Eng. Technol. 52, 797–801. https://doi.org/10.1016/j.net.2019.09.006.

Prävälie, R., Bandoc, G., 2018. Nuclear energy: Between global electricity demand, worldwide decarbonisation imperativeness, and planetary environmental implications. J. Environ. Manage. 209, 81–92. https://doi.org/10.1016/j.jenvman.2017.12.043.

Priddy, S.A., Hanley, T.R., 2003. Effect of agitation on removal of acetic acid from pretreated hydrolysate by activated carbon. Appl. Biochem. Biotechnol. - Part A Enzym. Eng. Biotechnol. 106, 353–364. https://doi.org/10.1385/ABAB:106:1-3:353.

Rattana, T., Chaiyakun, S., Witit-Anun, N., Nuntawong, N., Chindaudom, P., Oaew, S., Kedkeaw, C., Limsuwan, P., 2012. Preparation and characterization of graphene oxide nanosheets. Procedia Eng. 32, 759–764. https://doi.org/10.1016/j.proeng.2012.02.009.

Reife, A., Freeman, H.S., 1996. Environmental Chemistry of Dyes and Pigments.

Schacht, C., 2004. Refractories Handbook. CRC Press, Boca Rat.

Selvanantharajah, N., Iyngaran, P., Abiman, P., 2019. Quantitative studies of cadmium ion (Cd2+) adsorption on oxidized graphite powder. Mater. Today Proc. 23, 105–110. https://doi.org/10.1016/j.matpr.2019.07.701.

Sendra, C., Gabarrell, X., Vicent, T., 2007. Material flow analysis adapted to an industrial area. J. Clean. Prod. 15, 1706–1715. https://doi.org/10.1016/j.jclepro.2006.08.019.

Shiau, C.Y., Pan, C.C., 2004. Adsorption of basic dyes from aqueous solution by various adsorbents. Sep. Sci. Technol. 39, 1733–1750. https://doi.org/10.1081/SS-120030779.

Shittu, I., Achazhiyath Edathil, A., Alsaeedi, A., Al-Asheh, S., Polychronopoulou, K., Banat, F., 2019. Development of novel surfactant functionalized porous graphitic carbon as an efficient adsorbent for the removal of methylene blue dye from aqueous solutions. J. Water Process Eng. 28, 69–81. https://doi.org/10.1016/j.jwpe.2019.01.001.

Slejko, F.L., 1985. Adsorption Technology: A Step-by-step Approach to Process Evaluation and Application. Chem. Industries 222 https://doi.org/19 (1985).

Sophia, A., C., Lima, E.C., 2018. Removal of emerging contaminants from the environment by adsorption. Ecotoxicol. Environ. Saf. 150, 1–17. https://doi.org/10.1016/j.ecoenv.2017.12.026.

Sutphin, D.M., Sabin, A.E., Reed, B.L., 1990. International Strategic Minerals Inventory summary report. Tin. US Geol. Surv. Circ. 930. J.

Sykam, N., Jayram, N.D., Rao, G.M., 2018. Highly efficient removal of toxic organic dyes, chemical solvents and oils by mesoporous exfoliated graphite: Synthesis and mechanism. J. Water Process Eng. 25, 128–137. https://doi.org/10.1016/j.jwpe.2018.05.013.

Tarawou, T., Young, E., 2015. Intraparticle and Liquid film Diffusion Studies on the Adsorption of Cu 2+ and Pb 2+ Ions from Aqueous Solution using Powdered Cocoa Pod (Theobroma cacao). Int. Res. J. Eng. Technol. 2395. –56.

Taylor, H.A., 2000. Graphite, Natural. Kirk-Othmer Encycl. Chem. Technol. 12 https://doi.org/10.1002/0471238961.1401202120012512.a01.

Tsai, W.T., Chou, Y.H., 2004. Government policies for encouraging industrial waste reuse and pollution prevention in Taiwan. J. Clean. Prod. 12, 725–736. https://doi.org/10.1016/S0959-6526(03)00053-2.

Vorpahl, K.W., French, K.A., Jordan, P.T., Jurinski, N.B., 1976. Health Hazards from Oil, Soot and Metals at a Hot Forging Operation. Am. Ind. Hyg. Assoc. J. 37, 217–226. https://doi.org/10.1080/0002889768507445.

Wang, S., Wang, C., Ji, X., 2017. Towards understanding the salt-intercalation exfoliation of graphite into graphene. RSC Adv. 7, 52252–52260. https://doi.org/10.1039/c7ra07489a.

Wareing, A., Abrahamsen-Mills, L., Fowler, L., Grave, M., Jarvis, R., Metcalfe, M., Norris, S., Banford, A.W., 2017. Development of integrated waste management options for irradiated graphite. Nucl. Eng. Technol. 49, 1010–1018. https://doi.org/10.1016/j.net.2017.03.001.

Wiemes, L., Pawlowsky, U., Mymrin, V., 2017. Incorporation of industrial wastes as raw materials in brick's formulation. J. Clean. Prod. 142, 69–77. https://doi.org/10.1016/j.jclepro.2016.06.174.

Xian, H., Peng, T., Sun, H., Wang, J., 2015. The effect of thermal exfoliation temperature on the structure and supercapacitive performance of graphene nanosheets. Nano-Micro Lett. 7, 17–26. https://doi.org/10.1007/s40820-014-0014-4.

Yang, M.Z., Liu, G.X., L., P.S., 2014. Biosorption of Cadmium(II) from Aqueous Solution by Fruiting Body of Agaricus blazei Murill. Asian J. Chem. 7, 2567–2574.

Yang, K., Zhao, Z., Xin, X., Tian, Z., Peng, K., Lai, Y., 2019. Graphitic carbon materials extracted from spent carbon cathode of aluminium reduction cell as anodes for lithium ion batteries: Converting the hazardous wastes into value-added materials. J. Taiwan Inst. Chem. Eng. 104, 201–209. https://doi.org/10.1016/j.jtice.2019.09.012.

Yusuf, M., Elfghi, F.M., Zaidi, S.A., Abdullah, E.C., Khan, M.A., 2015. Applications of graphene and its derivatives as an adsorbent for heavy metal and dye removal: A systematic and comprehensive overview. RSC Adv. 5, 50392–50420. https://doi.org/10.1039/c5ra07223a.

Zamri, N.I., Zulmajdi, S.L.N., Daud, N.Z.A., Mahadi, A.H., Kusrini, E., Anwar, U., 2021. Insight into the adsorption kinetics, mechanism and thermodynamics of methylene blue from aqueous solution onto pectin-alginate-titania composite microparticles. SN Applied sciences 3, 222. https://doi.org/10.1007/s42452-021-04245-9.

Zhang, X.N., Mao, G.Y., Jiao, Y.B., Shang, Y., Han, Y.B., 2013. Adsorption of anionic dye on magnesium hydroxide coated pyrolytic biochar and reuse by microwave irradiation. Int. J. Environ. Sci. Technol. https://doi.org/10.1007/s13762-013-0338-5 http://.

Zhu, Y., Stoller, M.D., Cai, W., Velamakanni, A., Piner, R.D., Chen, D., Ruoff, R.S., 2010. Exfoliation of graphite oxide in propylene carbonate and thermal reduction of the resulting graphene oxide platelets. ACS Nano 4, 1227–1233. https://doi.org/10.1021/nn901689k.